Modulation of aromatase by natural compounds—A pharmacophore guided molecular modelling simulations

S. Rampogu [1], C. Park [1], M. Son [1], A. Baek, A. Zeb, G. Lee, K.W. Lee [*]

Division of Life Science, Division of Applied Life Science (BK21 Plus), Plant Molecular Biology and Biotechnology Research Center (PMBBRC), Research Institute of Natural Science (RINS), Gyeongsang National University (GNU), 501 Jinju-daero, Jinju 52828, Republic of Korea

ABSTRACT

Globally, breast cancer is one of the primary reasons of death noticed in women. Despite continuous efforts to formulate effective treatments, search to identify promising therapeutics is underway. Consequently, a drug with low toxicity, high efficacy, and which can escape resistance mechanism is in a high demand. Natural compounds are bestowed with several medicinal properties demonstrating low toxicity. Therefore, the current research focuses on the use of several plant- derived chemical compounds against aromatase, a validated drug target for breast cancer. Correspondingly, employing the known inhibitors, a 3D QSAR pharmacophore model was generated and was subsequently validated. Using the three-featured pharmacophore as the 3D query, the alkaloids, flavonoids, coumarins and the AfroDB were scrupulously examined to retrieve the compounds with inhibitory activities complemented by the pharmacophore model. The obtained compounds were subjected to molecular docking studies executed employing the Cdocker accessible on discovery studio v4.5. The resultant ideal poses from the largest cluster conferred with key reside interactions and higher dock scores than the reference and the Food and Drug Administration (FDA) approved drugs were escalated to molecular dynamics simulation studies conducted employing GROMACS v5.0.6 for 30 ns. Correspondingly, the Hits (ZINC95486358, ZINC95486354, and ZINC90711737) have displayed stable root mean square deviations, coupled by appropriate positioning at the active site displaying greater number of hydrogen bonds. Moreover, the Hits (ZINC95486358, ZINC95486354, and ZINC90711737) were noticed to anchor with various key residues essential for clamping the ligand at the binding pocket. Therefore, these findings guide us to determine that the identified Hits can act effectively against breast cancer, thereby increasing the life expectancy. Furthermore, they can assist as scaffolds for designing novel drugs that aid in curing the cancer.

© 2018 SAAB. Published by Elsevier B.V. All rights reserved.

1. Introduction

The enzyme aromatase is fundamentally essential for the conversion of androgens to aromatic estrogens executed through three hydroxylation reactions (Subramanian et al., 2008; Chen et al., 2009; Chan et al., 2015). This is a member of cytochrome P450 family of *CYP19A1* gene, located on chromosome 15 (Chumsri et al., 2011a). The key importance of aromatase is that it is the only enzyme in vertebrates capable of aromatizing the six-membered ring and consequently the only enzyme that generates estrogen (Chumsri et al., 2011b). This enzyme is predominantly observed in the ovaries, adipose fibroblast cells of the postmenopausal women and placenta of the pregnant women. The so formed estrogens demonstrate their actions after anchoring to their corresponding receptors such as the estrogen receptor-α and the estrogen receptor-β (Lubahn et al., 1993; Krege et al., 1998; Dupont

et al., 2000; Zhao et al., 2016). A significant role of estrogens is noticed in the female reproductive system (Bulun, 2005; Carroll, 2007), while plays an essential role in vascular biology (Mendelsohn, 2002; O'Lone et al., 2007; Knowlton and Lee, 2012), bone metabolism (Väänänen and Härkönen, 1996; Nakamura et al., 2007; Prior et al., 2017; Sozen et al., 2017), bone resorption (Riggs, 2000; Streicher et al., 2017; Tabatabaei-Malazy et al., 2017), brain and its functions (Gillies and McArthur, 2010; Zarate et al., 2017), in cognition (Cheon, 2017; Girard et al., 2017; Yan et al., 2017) and estrogen related α gene in binge eating (Lutter et al., 2017). Nevertheless, the estrogen has gained wider attention for its role in demonstrating breast cancer and several benign and malignant hormone-dependent disorders (Bulun, 2005; Santen et al., 2015).

The enzyme aromatase was observed to be in elevated levels in breast cancer women together with high levels of estrogen (Harada, 1997; Balunas et al., 2008). Furthermore, it is well established that estrogen exerts a striking ability of proliferation and is able to trigger the breast epithelial cell mitosis and promotes the cell divisions, paving way for random genetic errors (Travis and Key, 2003). Correspondingly,

the proliferative effect of the estrogen is demonstrated by sequential steps in response to the estrogen that regulates the cell differentiation (Clemons and Goss, 2001). Consequently, being the solo source of estrogen production particularly in postmenopausal women, it can be deduced that inhibiting aromatase can lead to diminished levels of estrogen. Furthermore, hindering the aromatase activity and attempting to reduce the estrogen levels might result in decreased growth of the cancer cells (Kang et al., 2018).

One of the effective treatments administered to the patients is the use of aromatase inhibitors (AIs) (Chumsri et al., 2011b). AIs can be categorized into steroidal and non-steroidal based upon their molecular skeleton (Adhikari et al., 2017). The type I steroidal inhibitors such as formestane and exemestane exhibit a high structural similarity with the substrate and further covalently bind to the aromatase resulting in an irreversible reaction (Kang et al., 2018). These inhibitors are referred to as suicide inhibitors as they are inactivated by its own effect, decomposing the aromatase after binding (Thompson and Siiteri, 1974; Hong and Chen, 2006; Chumsri et al., 2011a; Daldorff et al., 2017). On the contrary the non-steroidal type II inhibitors, such as fadrozole, vorozole, rogletimide, letrozole and anastrozole, interact with the heme group thereby impeding the androgen binding leading to a competitive inhibition of androgens. Moreover, the cancer cells have developed resistance against aromatase inhibitors thereby hampering the effective treatment (Miller and Larionov, 2012; Ma et al., 2015; Hanamura and Hayashi, 2017). These conditions pave way for the development and designing of new drugs with no side effects, whilst contributing to effective therapeutics.

Although the AIs have proven to be beneficial in the postmenopausal breast cancer patients (Chlebowski et al., 2009) are often regarded as effective first-line therapeutics (Chlebowski et al., 2009), and are reported to have certain grave side effects on bones, brain and the heart (Chlebowski et al., 2006; Goss et al., 2007; Sini et al., 2017). In order to overcome these side effects and further to render treatment with less toxic effects, the use of natural compounds as AIs has been markedly increasing (Balunas and Kinghorn, 2010a, 2010b).

For the current study, different natural compounds have been chosen to assess their effect against the enzyme aromatase. The compounds such as alkaloids and flavonoids has been obtained from NPACT(Mangal et al., 2013) a unique database dedicated to experimentally validated plant derived compounds with anticancer activities. The coumarins have been acquired according to the literature support (Musa et al., 2008; Venugopala et al., 2013; Lv et al., 2015) and chemical compound from African medicinal plants(Ntie-Kang et al., 2013) available from Zinc database (http://zinc.docking.org/catalogs/afronp). These compounds were subsequently prepared by examining for any duplicates, and were energy minimized before subjecting them to molecular docking studies.

For the current investigation, the protein target aromatase with the PDB code 3EQM bearing a resolution of 2.90 Å containing an innate natural substrate, androstenedione was chosen. The active site is marked 10 Å around the substrate for all the atoms that exist within the selected dimension. Additionally, the residues Arg 115, Trp 141, Arg 145, Arg 375 and Arg 435 were found to interact with the haem moiety. The enzyme aromatase is further comprised of 12 major α-helices labeled from A to L and 10 β-sheets, numerically labeled from 1 to 10, organized into one major and three minor sheets (Ghosh et al., 2009).

Therefore, the objective of the current study is to assess the molecular affinities of the naturally occurring compounds on aromatase to identify the potential inhibitor.

2. Materials and methods

2.1. Selection of the dataset compounds

The selection of the known inhibitors play an important role for the subsequent pharmacophore construction, utilized for retrieving novel compounds from various databases. For the current investigation, a dataset consisting of 36 compounds from different literatures (Browne et al., 1991; Numazawa et al., 1996; Sonnet et al., 1998; Luqman et al., 2012; Mayhoub et al., 2012; Yadav et al., 2015) were established which were further grouped into the training set compounds and the test set compounds. The formation of the training set is a principle event as it is employed in the generation of the pharmacophore. A training set should include the most active compounds as it is exploited to offer the features used for inhibition. Additionally, a training set should have a minimum of 16 structurally diverse compounds (Sakkiah and Lee, 2012), should exhibit a range of 4–5 orders of magnitude and should impart knowledge on structural and activities of the small compounds. For the current study, 16 compounds were rigorously sorted and were grouped into training set that have exhibited different structures and varied activity ranges from 0.015 nmol/L–7,834,296 nmol/L. Furthermore, these compounds were further classified based upon the activity ranges. Compounds with the activity values less than 500 nmol/L are referred to as most active compounds, compounds with the activity ranges between 500 nmol/L–10,000 nmol/L were labeled as moderately active compounds and the compounds with activity values greater than 10,000 nmol/L are referred to as inactive compounds. Correspondingly, their 2D structures were sketched employing ChemSketch (http://www.acdlabs.com) and were imported onto the discovery studio v4.5 (DS) for generating their 3D structures.

2.2. Pharmacophore generation

The 16 training set compounds were employed to build the pharmacophore model. In order to generate the most reliable and efficient pharmacophore, it is important to comprehend on the inhibitory chemical features present within the compounds that could trigger the therapeutics against breast cancer. Accordingly, the *Feature Mapping* protocol available on the DS was recruited to probe into the features required for inhibition with a minimum and the maximum number of features were selected as 0 and 5, respectively. The resultant findings were used to generate the pharmacophore model employing the *3D QSAR Pharmacophore Generation* module available with the DS considering the minimum and the maximum features as 0 and 5 respectively. Furthermore, the BEST algorithm was used to generate the conformation of lower energy at the uncertainty property value of 3 while retaining the other parameters at default values. Correspondingly, ten pharmacophore models were prompted and the best amongst them was chosen based upon the Debnath's analysis.

2.3. Validation of the pharmacophore model

The obtained pharmacophore model was validated to assess its ability in predicting the activity of the compounds in the same order as the experimental activity values. To evaluate the robustness of the model in discrimination the active compounds from the inactives and thereby, retrieving the active compounds from various databases and its statistical significance. The chosen pharmacophore was validated to determine its robustness employing three different approaches (Rampogu et al., 2018a) such as, test set method of validation, decoy set method of validation and the Fischer's randomization method.

The test set validation was performed to assess if the selected Hypo could establish the activities of the compounds as those experimentally determined. The compounds that comprise the test set were the diverse compounds selected form the dataset other than the training set compounds, demonstrating different structures and varied IC_{50} values. The decoy set method was conducted to analyze whether the Hypo was able enough to retrieve the active compounds from the external data set. The results were secured based upon the enrichment factor (EF) and the goodness of fit (GF) scores. The Fischer's randomization method was executed to evaluate the statistical significance of the model and to establish that it was not generated by chance.

2.4. Virtual screening for identifying the new lead candidates

The validated pharmacophore model was employed as a 3D query to screen different natural compounds and natural compound databases to retrieve novel compounds imbibed with all the chemical features represented by the pharmacophore model. A set of 50 alkaloids and 162 flavonoids were retrieved from the NPACT (http://crdd.osdd.net/raghava/npact/), a total of 47 coumarin compounds were obtained from various literatures and 885 compounds from the African medicinal plants were grouped accordingly and were recruited to screen the compounds. Accordingly, the *Pharmacophore Mapping* tool embedded with the DS was enabled to retrieve the compounds that mapped well with the pharmacophore. All the retrieved compounds were considered to be imbibed with the inhibitory activities. These compounds along with the most active compound from the training set hereinafter referred to as reference compound and the two FDA approved drugs, exemestane and letrozole, were chosen for a comparative study.

2.5. Molecular docking mechanism

Molecular docking is one of the superior methods to estimate the binding affinities between the protein and the ligands and additionally determines the binding mode of the ligands. For the current study, the Cdocker accessible on the DS was employed which operates on CHARMm forcefield. This is a grid based docking programme, where the protein is held rigid while the ligands are allowed to move. The results are evaluated based upon the -Cdocker interaction energies, the higher the energy value, the greater the affinity between the protein and the corresponding ligands (Rampogu and Rampogu Lemuel, 2016). The target protein for the current study that was chosen has aromatase with the PDB code 3EQM. Correspondingly, the protein was downloaded from the protein data bank (www.rcsb.org) and was further prepared by removing all the water molecules and by subsequent addition of the hydrogen atoms. The histidine protonation state was aligned as was observed with the crystal structure. Additionally, the binding site was designated 10 Å around the in-built cocrystal, labelling all the atoms within the specified range as the active site residues. Accordingly, the residues Arg115, Ala306, Asp309, Val370, Leu372, Met374 and Leu477 were deemed important. To affirm the docking protocol employed, the cocrystal ligand was docked into the protein active site. The results have generated an acceptable RMSD of 1.2 Å, Supplementary Fig. 1. The ligands obtained from the virtual screening process along with the reference and the FDA approved drugs were docked into the active site of the protein permitting the generation of 50 docked poses and were subsequently clustered. Moreover, to secure the best-docked pose, the ligand from the largest cluster demonstrating the highest -Cdocker interaction energies were manually examined for the hydrogen bond interaction with the key residues. The obtained binding poses were further escalated to molecular dynamics (MD) simulations to contemplate the reliability of the docked poses and to delineate on the behaviour of the small molecules at the proteins active site.

2.6. Molecular dynamic simulations

The obtained poses from the molecular docking were subjected to molecular simulation studies to unravel the molecular behaviour of the ligands at the active sites and further to assess the stability of the protein ligand complex recruiting GROMACS v5.0.6 (Van Der Spoel et al., 2005) using the CHARMm27 forcefield. The ligand topologies were procured from SwissParam (Zoete et al., 2011) and the systems were solvated in the dodecahedron box withTIP3P water model and counter ions. Subsequently, to dislodge any unwanted contacts that exist within the initial structures, 10,000 minimization steps were conducted employing the steepest descent algorithm with a maximum force being lower than 1000 kJ/mol. The minimized structures were thereafter subjected to double phased equilibration steps. The primary

phase of NVT equilibration was executed for 1 ns at 300 K using a V-rescale thermostat for monitoring constant temperature. The secondary phase of NPT equilibration was conducted for 1 ns using 1 bar Parrinello-Rahman barostat (Parrinello, 1981). Care should be taken that the protein backbone is placed rigid allowing the solvent molecules and the counter-ions to wobble. Furthermore, SETTLE (Miyamoto and Kollman, 1992) and LINCS (Hess et al., 1997) algorithms were recruited to constrain the geometry of water molecules and the bonds involving hydrogen atoms respectively, implementing the periodic boundary conditions. Particle Mesh Ewald (PME) (Darden et al., 1993) algorithm was used to compute the long-range electrostatic interactions and a cut off distance of 9 Å and 10 Å was used to regulate the Coulombic and Van der Waals interactions. The ensemble complex structures were escalated to MD simulations conducted for 30 ns saving the data for every 1 ps. The generated results were thoroughly contemplated employing the visual molecular dynamics (VMD) (Humphrey et al., 1996) and DS.

3. Results and discussion

3.1. Pharmacophore generation

A total of 16 training set compounds Fig. 1 with the activity values spanning between 0.015 nmol/L and 7,834,296 nmol/L that demonstrated diverse chemical structures and activity values were utilized to build the statistically significant pharmacophore model recruiting the in-built *3D QSAR Pharmacophore Generation* feature obtainable with the DS. For its accomplishment, it uses the Catalyst *HypoGen* algorithm (Rampogu et al., 2018a) to obtain pharmacophore models from a set of known ligands with their known biological activities. Furthermore, the module generates the pharmacophore models depending upon the ability of the ligands to fit onto the pharmacophore model. From the knowledge imparted by the *Feature Mapping* protocol, the hydrogen bond acceptor (HBA), hydrogen bond acceptor lipid (HBL), hydrogen bond donor (HBD), positive ionizable (POS) and ring aromatic (RA) have been chosen with the maximum interfeature distance as 2.97. Accordingly, 10 hypotheses were generated with divergent values as represented in Table 1. Upon thorough evaluation of the features rendered by ten hypotheses, the ring aromatic has consistently appeared with all the hypothesis inferring its significance in contributing to the inhibitory activities. The best pharmacophore was chosen based upon the Debnath's analysis (Debnath, 2002), which states that the best pharmacophore model should exhibit a maximum cost difference, least RMSD, highest correlation with a substantial fit value.

Correspondingly, a pharmacophore model with three features, HBA, HBL and RA has been generated, Fig. 2A. Furthermore, upon superimposition of the active and the inactive compounds from the training set, it was observed that the active compound has aligned absolutely with all the features, Fig. 2B, while the inactive compound has mapped with two features of the Hypo1, Fig. 2C. Therefore, these findings suggest that the Hypo1 could ably differentiate the active compounds from the inactive ones.

To further evaluate the predictive ability of Hypo1, it was employed to assess the activities of each compound present in the training set by regression analysis. The results have demonstrated that the Hypo1 has efficiently predicted the activities of the compound in the same order of magnitude as the experimental results. However, one inactive compound was estimated as active compound. This demonstrates the ability of Hypo1 in estimating the activities of the compounds as their experimental ranges, Table 2.

3.2. Pharmacophore validation

The primary role of the selected Hypo1 is to retrieve the compounds from the databases with the inhibitory features similar to that of the active training set compounds; therefore, it is extremely essential to assess the robustness of the Hypo1. Accordingly, the chosen Hypo1
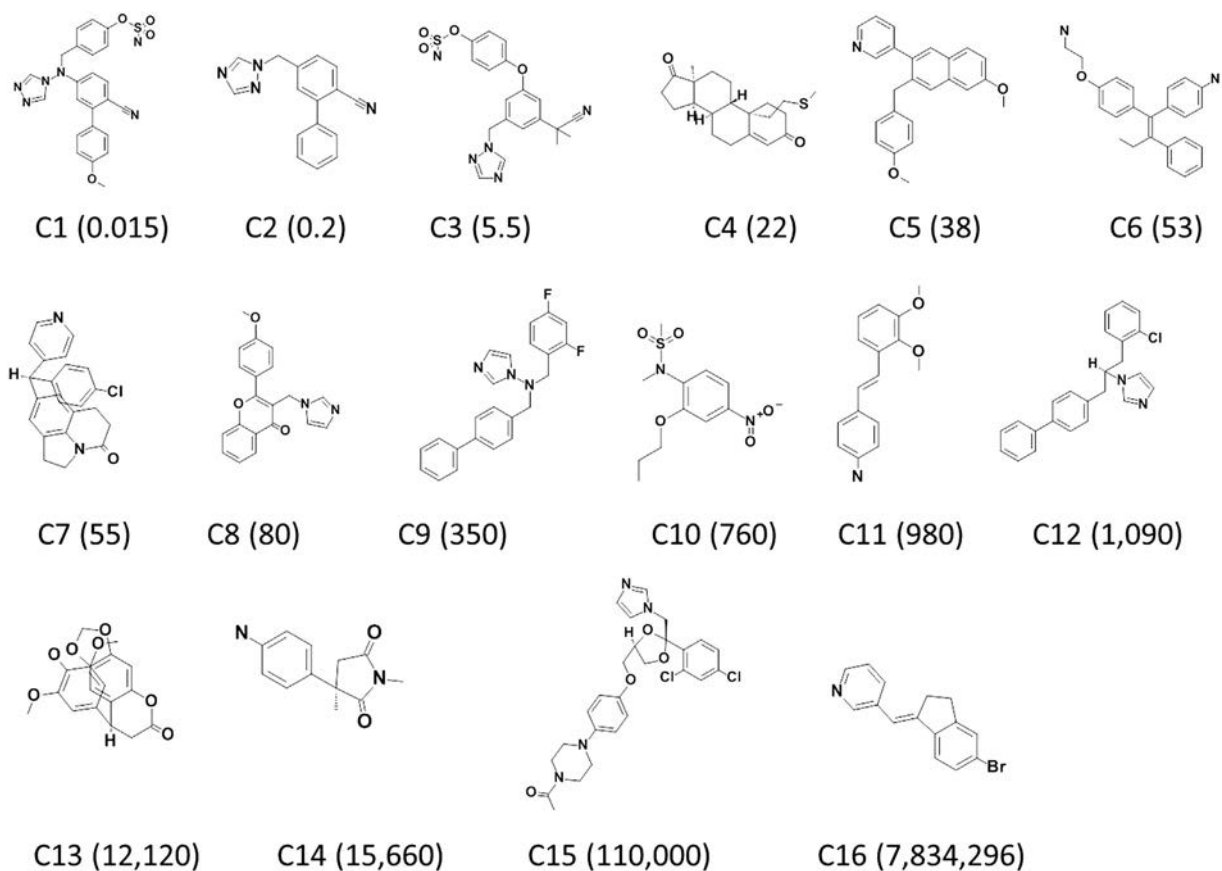
Fig. 1. 2D representation of the training set compounds.

was validated employing the Fischer's randomization method, test set method and the decoy set method.

3.2.1. Fischer's randomization method

To examine the statistical significance of the Hypo1, the Fischer's randomization was conducted at the confidence level 95% employing the formula $S = [1 - \frac{1+X}{Y}]X100$. In the equation, X refers to the total number of hypotheses bearing the cost lesser than Hypo X, and Y refers to the sum of the *HypoGen* runs (initial + random). The 95% confidence was attained when X = 0 and Y = 19 + 1, therefore, $S = [\frac{1+0}{19+1}]X\ 100 = 95$. Subsequently generated results, Fig. 3A, precisely indicate that the cost value of the Hypo1 was far lower than the 19 randomly generated spreadsheets. Furthermore, these results highlight the superior quality of the Hypo1 by additionally portraying that the Hypo1 was not generated by chance.

3.2.2. Test set method

Test set method was executed to assess if the Hypo1 could predict the activities of the compounds same as the experimental activity ranges upon employing the protocol used for training set compounds. A group of 20 compounds other than the training set compounds possessing different activity values were chosen for its execution. The compounds were further grouped depending upon their activity ranges. The compounds with activity values less than 500 nmol/L are referred to as most active compounds, compounds with the activity ranges between 500 nmol/L–10,000 nmol/L are labeled as moderately active compounds and the compounds with activity values greater than 10,000 nmol/L are referred to as inactive compounds, respectively. Hypo1 was able to predict the activities of the compounds in the same order of magnitude as noticed with the experimental ranges, however, one active and one inactive compound were determined as inactive and active compounds, correspondingly, Table 3. Furthermore, the

Table 1

Statistical parameters of ten pharmacophore hypotheses generated by *HypoGen*.

Hypo no	Total cost	Cost difference[a]	RMSD[b]	Correlation	Features[c]	Max fit
Hypo1	106.73	81.40	2.34	0.87	HBA, HBL, RA	10.78
Hypo2	106.75	81.38	2.37	0.87	HBL, HBL, RA	10.66
Hypo3	106.86	81.27	2.38	0.87	HBA, HBL, RA	10.61
Hypo4	107.09	81.04	2.37	0.87	HBL, HBL, RA	10.68
Hypo5	107.25	80.87	2.44	0.86	HBL, HBL, RA	10.36
Hypo6	107.45	80.68	2.43	0.86	HBA, HBA, RA	10.45
Hypo7	107.48	80.65	2.41	0.86	HBA, HBA, RA	10.56
Hypo8	109.97	78.16	2.52	0.85	HBA, HBL, RA	10.35
Hypo9	110.60	77.53	2.49	0.86	HBA, HBL, RA	10.66
Hypo10	110.91	81.38	2.55	0.85	HBA, HBL, RA	10.38

[a] Cost difference, difference between the null cost and the total cost. The null cost, the fixed cost and the configuration cost are 188.138, 56.8887and 12.03, respectively.
[b] Root mean square deviation.
[c] Abbreviation used for features: HBA, hydrogen bond acceptor; HBL, hydrogen bond acceptor Lipid; RA, ring aromatic.
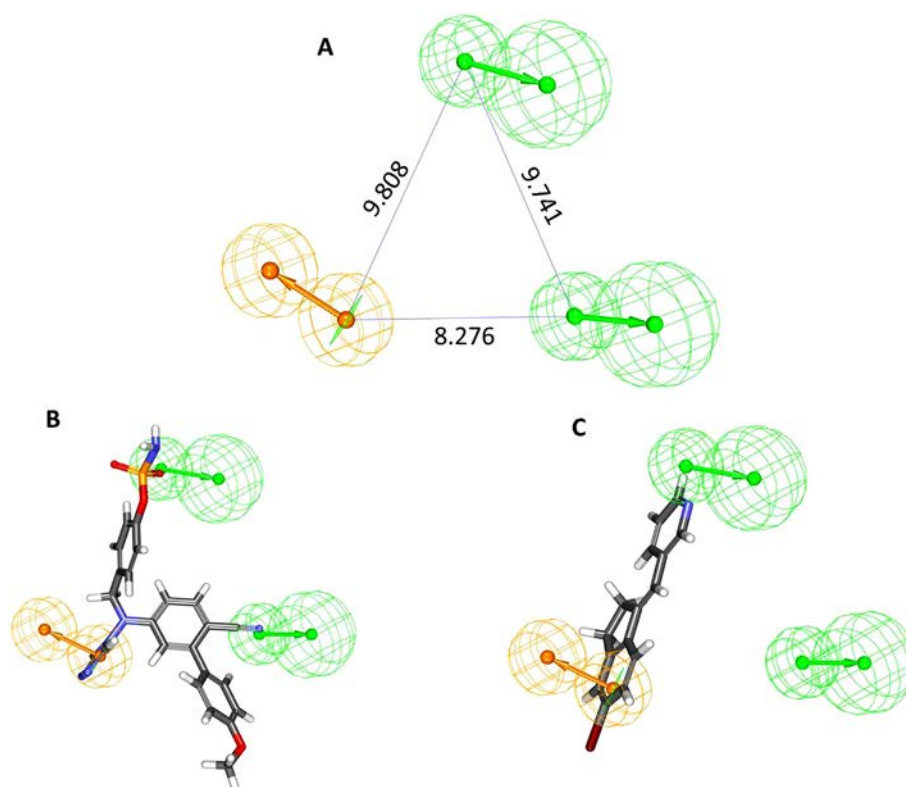
Fig. 2. A) Interfeature distance of the generated three-featured pharmacophore, B) Mapping of the most active compound from the training set is found to abide to all the features of the pharmacophore. C) Aligning of the inactive compound from the training set shows that only two features are been mapped.

linear regression of the test set compounds was computed to be 0.87, demonstrating a greater correlation between the experimental and the predicted activities of test set and the training set, Fig. 3B.

3.2.3. Decoy set method

The decoy set method was employed to assess the ability of the pharmacophore in selecting the active compounds from an external dataset. Correspondingly, a dataset (D) of 152 compounds was

organized comprising of 40 active compounds. The *Ligand Pharmacophore Mapping* protocol was subsequently launched and the obtained results were assessed based upon the goodness of fit score (GF) and the enrichment factor (EF). These parameters were computed using the formula,

$$EF = \left(\frac{Ha}{Ht}\right) \div \left(\frac{A}{D}\right)$$

$$GF = \left[\left(\frac{Ha}{4HtA}\right)(3A + Ht) \times [1 - (Ht - Ha) \div (D - A)]\right]$$

The quality of the model was estimated depending upon the GF score, which lies between 0 to 1 quantifying the model to be between null, and ideal. Accordingly, Hypo1 has mapped to 43 compounds (Ht) with 36 actives (Ha) in it. Moreover, the GF score was computed as 0.77, extrapolating the model to be a good one (Rampogu et al., 2017). The obtained findings illuminate the ability of the pharmacophore in retrieving the compounds with inhibitory effect from an external dataset. The details of the decoy set calculations are summarized in Table 4.

3.3. Virtual screening of the databases

Virtual screening using the validated pharmacophore as the 3D query is one of the significant approaches in retrieving the chemical compounds from the databases. Logically, the chemical features imbibed by the Hypo1 display as crucial role in identifying the compounds with similar inhibitory activities. Correspondingly, the validated Hypo1 was utilized to screen the databases such as the alkaloids, flavonoids, AfroDB and coumarins, employing the *Ligand Pharmacophore Mapping* module embedded on the DS. The Hypo1 was allowed to map with and subsequently redeem the compound. Consequently, 10 alkaloids, 61 flavonoids, 109 compounds from AfroDB, and 7 coumarins have

Table 2

Experimental and predicted activities of the training set molecules based on the pharmacophore model Hypo1.

Name	Fit value[a]	IC$_{50}$(nmol/L)		Error[b]	Activity scale	
		Experimental	Predicted		Experimental	Predicted
C1	10.25	0.015	0.025	1.7	+++	+++
C2	7.14	0.2	32	160	+++	+++
C3	6.84	5.5	65	12	+++	+++
C4	6.72	22	85	3.9	+++	+++
C5	6	38	45	3.9	+++	+++
C6	6.12	53	45	3.9	+++	+++
C7	7.07	55	38	−1.5	+++	+++
C8	5.03	80	48	−1.5	+++	+++
C9	6.6	350	110	−3.1	+++	+++
C10	5.29	760	2300	3	++	++
C11	5.2	980	2800	2.8	++	++
C12	5.83	1100	660	−1.6	++	++
C13	5.98	12,000	470	−26	+	+++
C14	3.6	16,000	110,000	7.2	+	+
C15	5.35	110,000	2000	−56	+	++
C16	3.6	7.800000	110,000	−69	+	+

[a] Fit value indicates how well the features in the pharmacophore overlap the chemical features in the molecule.

[b] Division of higher value of experimental or predicted IC50 by lower predicted or experimental IC50 value. '+' indicates that the predicted IC50 is higher than the experimental IC50; '−' indicates that the predicted IC50 is lower than the experimental IC50; a value of 1 indicates that the predicted IC50 is equal to the experimental IC50.

A. Fischer's randomization
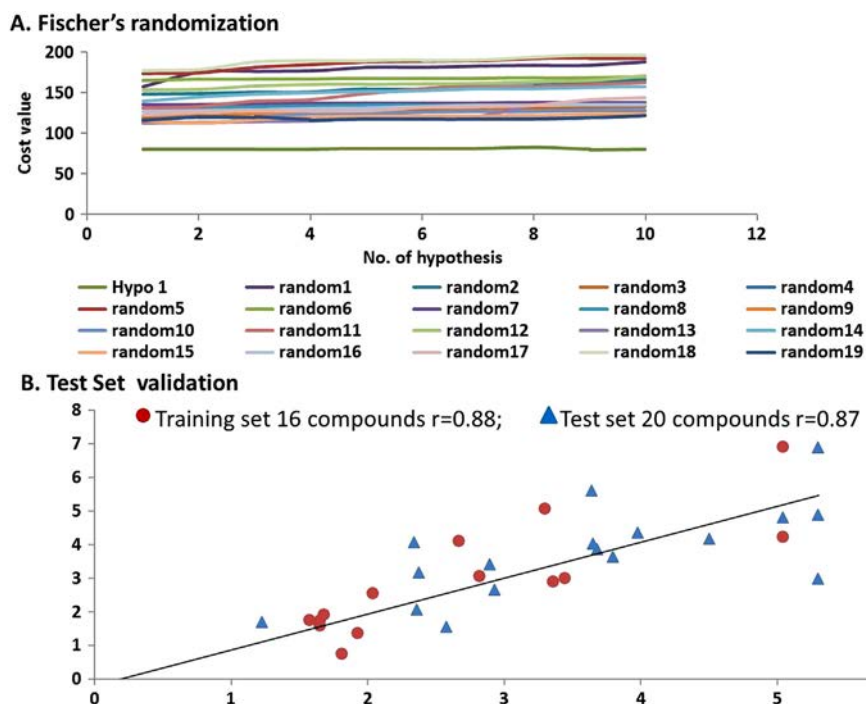

B. Test Set validation

Fig. 3. Validation of the pharmacophore model, A) Fischer's randomization illustrates that Hypo1 has the least cost value. B) Test set validation depiction where the regression is in harmony with the training set.

aligned with the Hypo1. The resultant 187 compounds were escalated to molecular docking studies to delineate on the interactions of these compounds at the protein active site and additionally to secure an ideal binding mode.

3.4. Molecular docking studies

Molecular docking is one of the techniques employed to sample the conformations of small molecules at the protein active site using different scoring functions. For the current study, the Cdocker available with the DS was employed to conduct the molecular docking studies. The

filtered 187 compounds along with the reference (most active compound in the training set) and two FDA approved drugs were upgraded to docking at the specified parameters as described previously, Supplementary Fig. 1. For the selection of the most valuable candidate compounds, all the compounds that have rendered a dock score higher than the reference compound and the FDA approved drugs were considered for further processing. Accordingly, the compounds from the largest cluster that demonstrated an ideal binding mode, with highest dock score complemented by key residue interactions were sorted. A total of 19 compounds have satisfied the above criteria and were referred to as potential Hits, Table 5. It was noteworthy to observe that the flavonoids and the AfroDB have rendered highest dock score than the reference and approved drugs, Table 5. Amongst them, three highest dock scored compounds that have represented interactions with the key residues and additionally mapped with all the features of the pharmacophore, Fig. 5, were labeled to as Hits. These compounds were subjected to molecular dynamics studies to delineate on the nature of the ligands at the proteins' active site and further to estimate and authenticate the docking accuracy.

3.5. Molecular dynamics simulations

To further shed light and gain insight into the behaviour of the small molecules at the proteins active site and to assess their stability thereby

Table 3
Experimental and predicted IC50 values of test set molecules as evaluated by Hypo1.

Name	Fit	IC$_{50}$(nmol/L)		Error[a]	Activity scale	
		Experimental	Predicted		Experimental	Predicted
C1	8.61	0.05	0.52	10	+++	+++
C2	8.17	0.15	1.4	9.5	+++	+++
C3	8.04	0.51	1.9	3.7	+++	+++
C4	5.74	34	380	11	+++	+++
C5	7.1	47	17	−2.8	+++	+++
C6	5.96	110	230	2.1	+++	+++
C7	5.39	440	460	1.9	+++	+++
C8	3.02	910	200,000	220	++	+
C9	5.93	1400	540	−5.8	++	++
C10	5.42	2500	790	−3.2	++	++
C11	4.52	4200	6300	1.5	++	++
C12	4.64	6900	4800	−1.4	++	++
C13	4.67	10,000	4500	−2.2	++	++
C14	5.97	11,000	220	−49	+	+++
C15	3.82	14,000	32,000	2.3	+	+
C16	4.34	22,000	9600	−2.3	+	++
C17	3.29	61,000	110,000	1.8	+	+
C18	3.02	72,000	200,000	2.8	+	+
C19	4.68	380,000	44,000	−88	+	+
C20	3.02	7.40E + 06	200,000	−37	+	+

[a] '+' indicates that the predicted IC50 is higher than the experimental IC50; '−' indicates that the predicted IC50 is lower than the experimental IC50; a value of 1 indicates that the predicted IC50 is equal to the experimental IC50.

Table 4
Different parameters calculated in decoy set method.

Parameters	Values
Total number of molecules in database (D)	152
Total number of actives in database (A)	40
Total number of Hit molecules from the database (Ht)	43
Total number of active molecules in Hit list (Ha)	36
% Yield of active [(Ha/Ht)]	83.72
% Ratio of actives [(Ha/A) × 100]	90
Enrichment factor (EF)	3.18
False negatives (A–Ha)	4
False positives (Ht–Ha)	7
Goodness of fit score (GH)	0.77

Table 5
Potential Hits and their respective dock scores.

Compound Name	-Cdocker energy	-Cdocker interaction energy
ZINC95486358	13.99	64.36
ZINC95486354	23.31	57.71
ZINC90711737	11.31	57.29
ZINC95486309	22.25	56.67
ZINC95486171	13.08	56.18
ZINC95486056	30.97	56.05
ZINC95486340	24.19	54.75
ZINC95486124	21.57	54.37
ZINC01530009	45.924	53.15
ZINC95485961	− 5.67	52.49
Curcumin	30.32	52.39
Puerarin	6.31	43.78
Myricetin 3-O-beta-glucuronide	34.82	40.75
Isorhamnetin 3-O-beta-D-glucopyranoside	24.83	40.20
Gericudranin	15.52	36.60
Apigenin-7-O-beta-D-glucopyranoside	21.21	36.31
Baicalin	12.20	35.00
Myricetin 3-O-alpha-rhamnoside	29.69	33.29
Gericudranin C	17.85	26.34
Letrozole	8.716	19.05
exemestane	64.20	13.90
Reference	87.33	8.54

-Cdocker energy and -Cdocker interaction energy are expressed in kcal/mol.

ensuring the reliability of the docking results, the molecular dynamics simulations were executed recruiting GROMACS to accomplish this endeavor. A 30 ns MD run was initiated and the findings were read by means of root mean square deviation (RMSD) for the protein backbone atoms. The RMSD values were noticed to be less than 0.2 nm for all the four systems, Fig. 4A, throughout the simulations inferring that the systems were in harmony with no abnormal behaviour. Additionally, the average RMSD for the reference was observed to be 0.18 nm while Hit1, Hit2 and Hit3 were found to be 0.16 nm, 0.14 nm and 0.14 nm, correspondingly. These results imply that the Hits were relatively stable than the reference throughout the whole simulation. Following this, to probe into the binding mode analysis, the representative structures

from the last 4 ns trajectories were extracted and were thereafter superimposed. The superimposition revealed that the Hits have displayed a binding pattern similar to that of the reference, Fig. 4B being seated at the active site. Monitoring the intermolecular interactions, it was disclosed that a good number of key residues have anchored with the ligands establishing proper positing of the ligands.

Delineating on the reference compounds it was observed that the reference has formed five hydrogen bond interactions involving the residues Asp371, Leu372, Met374, and Leu477, respectively rendered by an acceptable bond length, Fig. 5A. Additionally, a host of charged residues have facilitated the accommodation of the ligand in the active site. The residues Val370, Leu372, Asp309, and Ser478 have held the ligand through the carbon hydrogen bonds. The Met374 residue has displayed a unique π-sulfur bond rendered by 5.6 Å with the benzene ring A of the ligand. The aromatic ring of Phe134 has interacted with the ring A of the ligand forming a π–π T shaped bond with a distance of 4.5 Å. The benzene ring of Phe221 has joined with ring C of the ligand rendered by a distance of 5.4 Å forming π–π T stacked interaction. Additionally the pentane ring of the reference compound has interacted with Ile133, Ile305, and Ala306 firmly holding the ligand through π–alkyl interactions. Moreover, different charged amino acid residues such as Arg115, Trp224, Glu302, Thr310, Val369, Val373, and Ile395 were noticed to interact with the ligand through various Van der Waals interactions, Table 6 and Supplementary Fig. 2.

The Hit1 has formed four hydrogen bond interactions rendered by three residues, Arg115, Leu372 and Leu477, respectively, by a bond distance lower than 3 Å, Fig. 5B. Additionally, the ring A of the ligand has joined to the aromatic ring of Phe221 forming a π–π T interaction rendered by a distance of 3.8 Å. Similar interaction was noticed with the imidazole ring of His480 and the ring A of ligand with a distance of 4.8 Å demonstrating π–π T interaction. The benzene ring of the Trp224 residue has interacted with the ring B of Hit1 with a distance of 5.8 formed by π–π T interaction. These interactions were held at the extreme ends of the ligand and thereby locking the Hit1 into the proteins binding pocket. The residues Ile133 and Val313 were noticed to contribute towards proper positioning of the ligand formed by π–alkyl interactions holding the ligand at ring A and ring B, respectively. Alternatively, the residues Leu372, Leu477 and Ser478 were involved in the interactions through carbon hydrogen bonds. The charged residues
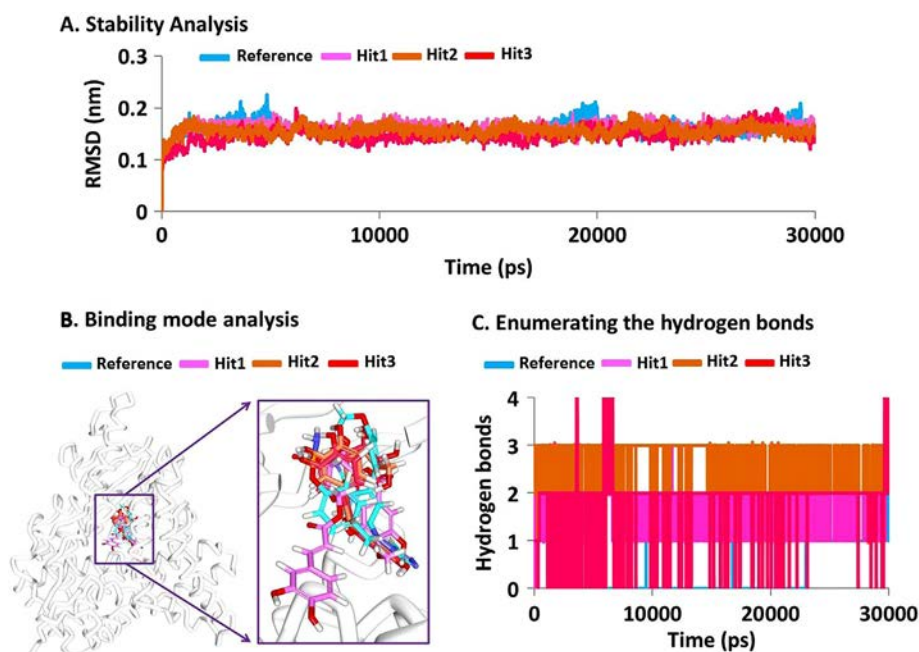

Fig. 4. Molecular dynamics simulation results. A) Illustration of the stability of the protein backbone atoms. The RMSD appears to be stable for all the systems. B) Accommodation of the Hits and the reference within the binding pocket. C) Enumeration of the hydrogen bonds, the Hits have rendered greater number of hydrogen bonds than the reference.
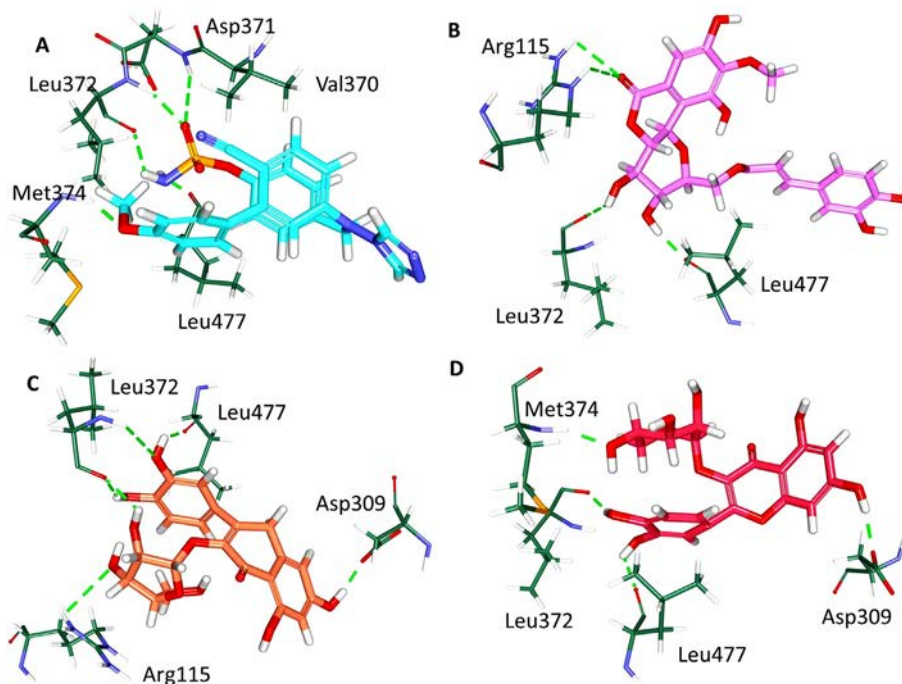
Fig. 5. Molecular hydrogen bonds of the reference (A), Hit1 (B), Hit2 (C) and Hit3 (D), respectively.

such as Arg192, Phe134, Gln218, Ser478, Pro481, Glu483 have formed the Van der Waals interactions aiding the ligand to be accommodated within the binding pocket, Table 6 and Supplementary Fig. 3.

Hit2 has formed the highest number of hydrogen bonds summing to six involving four residues, Arg115, Asp309, Leu372 and Leu477,

Table 6
Comprehensive molecular interactions between proteins key residues and the ligands.

Name	Hydrogen bond interactions <3 Å	π-Bonds	Alkyl/π-alkyl	Van der Waals interactions
Ref	Asp371:HN-O31 (2.9)	Phe134, Phe221	Ile133,	Arg115, Trp224,
	Leu372:HN-O31 (2.0)		Ile305,	Glu302, Thr310,
	Met374:HN-O33 (1.9)		Ala306	Val369, Val373,
	Leu477:O-H50 (1.8)			Ile395
Hit1	Arg115:HE-O39 (2.9)		Ile133, Val313	Arg192, Phe134,
	Arg115:HH21-O39 (2.7)	Phe221,Trp224,		Gln218, Ser478,
	Leu372:O-H56 (2.3)	His480		Pro481, Glu483
	Leu477:O-H55(1.9)			
Hit2	Arg115:HH1-O32 (2.9)	–		
	Asp309:OD2-H42 (1.8)		Ile133,	
	Leu372:HN-O34 (2.8)		Trp224,	Ile105, Phe134,
	Leu372:O-H51(2.0)		Ala306,	Phe221,Asp371,
	Leu372:O-H49 (2.0)		Val370,	Met374,Ser478
	Leu477:O-H50(1.9)		Leu477	
Hit3	Asp309:OD2-H41 (1.8)	–	Ile133,	
	Leu372:O-H49 (1.8)		Ala306,	Phe134, Phe221,
	Met374:HN-O31 (1.9)		Val370,	Trp224, Asp371, Ser478
	Leu477:O-H48 (2.0)		Leu477	

respectively demonstrating an acceptable bond length, Fig. 5C. Additionally, the residues Arg115 and Val373 have involved with the ligand by forming the carbon–hydrogen bonds. Unlike other ligands, the Hit2 was devoid of π–π T interaction, however, formed alkyl and π–alkyl interactions. The ring A of the ligand has interacted with the Ala306 and Ile133 of the protein with the π–alkyl interactions. The ring B of the ligand has interacted with Trp224 by π–alkyl and Val370 residue by alkyl hydrophobic bond. Furthermore, the ring C has anchored to Val370 and Leu477 by π–alkyl interactions. These interactions further lead us to understand that the alkyl and π–alkyl interactions were spread across the ligand thereby effectively clamping the ligand. Additionally, the Van der Waals interaction formed by the residues Ile105, Phe134, Phe221, Asp371, Met374, and Ser478 further assist the ligand to be buried into the active site, Supplementary Fig. 4.

The Hit3 has formed four hydrogen bond interactions with the key residues Asp309, Leu372, Met374 and Leu477 contributed by an acceptable bond length, Table 6 and Fig. 5D. The residues Leu372, Val370, and Val373 have involved in the molecular interaction with the carbon hydrogen bonds. Furthermore, the π–alkyl interactions were noticed with the rings A, B and C of the ligand formed by different residues. Ile133 and Ala306 residues held the ring A while the ring B is held by Val370 residue. Furthermore, the ring C has participated in the π–alkyl interactions with Val370 and Leu477 residues thereby firmly positioning the ligand. Besides these, the charged residues such as Phe134, Phe221, Trp224, Asp371, and Ser478 substantially locked the inhibitor within the active site of the protein, Supplementary Fig. 5.

To further decipher on the nature of the binding of the candidate compounds at the active site of the protein, their intermolecular hydrogen bond interactions were scrupulously monitored throughout the simulation time. The average hydrogen bonds noted for the reference compound was recorded as 0.4 while the Hit1, Hit2 and Hit3 has generated 1.7, 2.4 and 1.9, respectively, Fig. 4C. These results together with the comprehensive interactions distinctly illuminate the superiority of the Hit compounds over the reference compound and guide us to comprehend on employing the natural compounds against aromatase. The Hits have additionally revealed the features demonstrated by the Hypo1, bestowed by aligning well with the pharmacophore model, Fig. 6. Furthermore, the novelty of the identified Hits was assessed
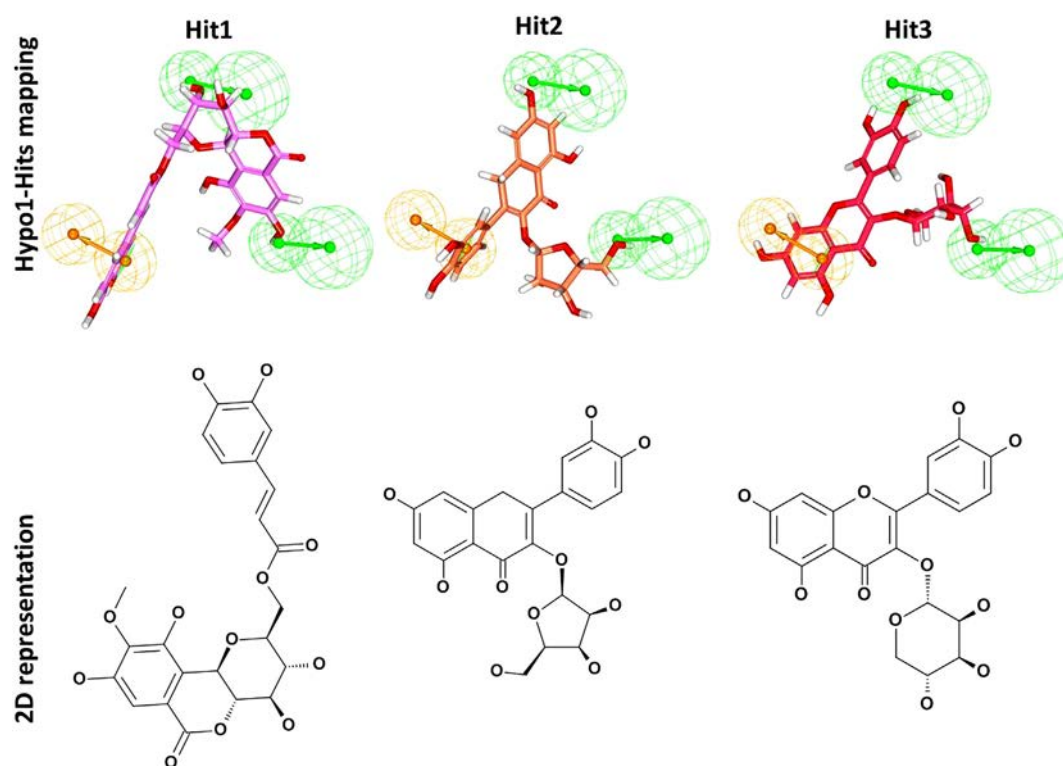
Fig. 6. Overlay of the Hits onto the Hypo1 displayed that the Hits represent the key features essential for inhibition.

using the online search tool such as PubChem and the results assured the novelty of the compounds.

4. Discussion

Estrogen plays an important role noticed in the hormone-dependent breast cancer proliferation with an elevated levels (Brueggemeier et al., 2001; Ahmad and Shagufta, 2015). In the recent years, two approaches have been deduced to combat this, which includes development of estrogen receptor antagonist, or to develop new drugs against breast cancer (Maurizio et al., 2002; Park and Jordan, 2002; Miller, 2004). Natural compounds are deemed to have several medicinal values and have been assisting the humankind from ancient ages (Dias et al., 2012; Uysal et al., 2016; Zengin et al., 2018). The use of natural compounds as potential AIs have proven to be promising therapeutics as they are non-toxic and abundant in availability (Balunas et al., 2008; Balunas and Kinghorn, 2010a, 2010b; Mocanu et al., 2015). Accordingly, the current investigation proceeds with the generation of 3D QSAR pharmacophore model and to subsequently obtain the compounds with inhibitory groups. The pharmacophore methods for the identification of lead compounds have been in a great demand in the drug discovery pipeline and have been well documented (Langer and Hoffmann, 2006; Katsila et al., 2016; Rai et al., 2017; Ma et al., 2018; Rampogu et al., 2018b). Encouraged by these reports, the current investigation proceeds by *in silico* methods to retrieve the potential compounds from different phytochemicals.

The well-validated pharmacophore model, Hypo1 was employed to screen and subsequently identify the compounds with inhibitory potential. Amongst the retrieved compounds, the natural compounds have generated higher dock scores than the known drugs, illuminating their therapeutic potential. The compounds from the Zinc database have rendered significantly higher dock scores, being accommodated at the active site of the protein with several key residues as was noticed earlier (Mirzaie et al., 2013). It was worth mentioning that the Hit1 has anchored with the key residue Arg115, and Hit2 has joined with the key residues such as Asp309 and Arg115, while Hit3 interacted with

Met374, respectively. These interactions are in agreement with the previously reported results. (Mirzaie et al., 2013; Lee and Barron, 2018). Additionally, the MD affirmed docking results have revealed that the residues Leu372 and Leu477 have formed the hydrogen bonds with all the Hits as was observed with the reference rendered by acceptable bond length and are in parallel with the previous reports (Kumavath et al., 2016). The residues such as Ile133 and Phe134 were observed with the Hits forming the Alkyl/π–alkyl and Van der Waals interactions, respectively, holding the ligand firmly at the active site groove.

The residues Ile133 and Phe134 were noticed to interact with the ligands from one side while the Leu372 and Leu477 were located at the opposite site thereby clamping the ligands firmly at the protein active site. These observations direct us to assume that the interactions with the residues Ile133, Phe134, Leu372 and Leu477 are imperative in inducing the therapeutic potential. Furthermore, these findings prompt us to speculate that the identified Hit candidates might potentially exert aromatase suppression.

5. Conclusion

The current study emphasizes the use of natural compounds against breast cancer. Breast cancer is regarded as one of the major causes of death in women noticed globally. The currently available treatments have manifested several toxic effects with the association of resistance that provokes the urgency in the development of new drugs. Natural compounds have been known to be possessed with medicinal properties since the ancient period. For the current investigation, different natural compounds have been evaluated to assess their efficacy against aromatase using computational approaches. The chosen natural compounds have generated higher dock scores than currently available treatments thereby emphasizing there usability as alternative therapeutics. Additionally, the identified Hit compounds (ZINC95486358, ZINC95486354, and ZINC90711737) have demonstrated key interactions complemented by an ideal binding mode with stable MD results as compared with the reference compound. Therefore, we presume

that these compounds could act as potential alternatives to breast cancer or can serve as platforms for designing new drugs.

Appendix A. Supplementary data

Supplementary data to this article can be found online at https://doi.org/10.1016/j.sajb.2018.06.019.

References

Adhikari, N., Amin, S.A., Saha, A., Jha, T., 2017. Combating breast cancer with non-steroidal aromatase inhibitors (NSAIs): understanding the chemico-biological interactions through comparative SAR/QSAR study. European Journal of Medicinal Chemistry 137:365–438. https://doi.org/10.1016/j.ejmech.2017.05.041.

Ahmad, I., Shagufta, 2015. Recent developments in steroidal and nonsteroidal aromatase inhibitors for the chemoprevention of estrogen-dependent breast cancer. European Journal of Medicinal Chemistry 102:375–386. https://doi.org/10.1016/j.ejmech.2015.08.010.

Balunas, M.J., Kinghorn, A.D., 2010a. Natural compounds with aromatase inhibitory activity: an update. Planta Medica https://doi.org/10.1055/s-0030-1250169.

Balunas, M.J., Kinghorn, A.D., 2010b. Natural product compounds with aromatase inhibitory activity: an update. Planta Medica 76:1087–1093. https://doi.org/10.1055/s-0030-1250169.

Balunas, M.J., Su, B., Brueggemeier, R.W., Kinghorn, A.D., 2008. Natural products as aromatase inhibitors. Anti-Cancer Agents in Medicinal Chemistry 8:646–682. https://doi.org/10.1016/j.phytol.2009.11.005.The.

Browne, L.J., Gude, C., Rodriguez, H., Steele, R.E., Bhatnager, A., 1991. Fadrozole hydrochloride: a potent, selective, nonsteroidal inhibitor of aromatase for the treatment of estrogen-dependent disease. Journal of Medicinal Chemistry 34:725–736. https://doi.org/10.1021/jm00106a038.

Brueggemeier, R.W., Richards, J.A., Joomprabutra, S., Bhat, A.S., Whetstone, J.L., 2001. Molecular pharmacology of aromatase and its regulation by endogenous and exogenous agents. Journal of Steroid Biochemistry and Molecular Biology:75–84 https://doi.org/10.1016/S0960-0760(01)00127-3.

Bulun, S.E., 2005. Regulation of aromatase expression in estrogen-responsive breast and uterine disease: from bench to treatment. Pharmacological Reviews 57:359–383. https://doi.org/10.1124/pr.57.3.6.

Carroll, R.G., 2007. 14 — female reproductive system. In: Carroll, R.G. (Ed.), Elsevier's Integrated Physiology. Mosby, Philadelphia:pp. 177–187 https://doi.org/10.1016/B978-0-323-04318-2.50020-0.

Chan, H.J., Petrossian, K., Chen, S., 2015. Structural and functional characterization of aromatase, estrogen receptor, and their genes in endocrine-responsive and -resistant breast cancer cells. The Journal of Steroid Biochemistry and Molecular Biology 161:1–11. https://doi.org/10.1016/j.jsbmb.2015.07.018.

Chen, D., Reierstad, S., Lu, M., Lin, Z., Ishikawa, H., Bulun, S.E., 2009. Regulation of breast cancer-associated aromatase promoters. Cancer Letters https://doi.org/10.1016/j.canlet.2008.05.038.

Cheon, S., 2017. Hippocampus-dependent task improves the cognitive function after ovariectomy in rats. Osong Public Health and Research Perspectives 8:227–234. https://doi.org/10.24171/j.phrp.2017.8.3.10.

Chlebowski, R.T., Anderson, G.L., Geller, M., Col, N., 2006. Coronary heart disease and stroke with aromatase inhibitor, tamoxifen, and menopausal hormone therapy use. Clinical Breast Cancer 6. https://doi.org/10.3816/CBC.2006.s.005.

Chlebowski, R., Cuzick, J., Amakye, D., Bauerfeind, I., Buzdar, A., Chia, S., Cutuli, B., Linforth, R., Maass, N., Noguchi, S., Robidoux, A., Verma, S., Hadji, P., 2009. Clinical perspectives on the utility of aromatase inhibitors for the adjuvant treatment of breast cancer. The Breast 18:S1–S11. https://doi.org/10.1016/S0960-9776(09)70002-5.

Chumsri, S., Howes, T., Bao, T., Sabnis, G., Brodie, A., 2011a. Aromatase, aromatase inhibitors, and breast cancer. The Journal of Steroid Biochemistry and Molecular Biology 125:13–22. https://doi.org/10.1016/j.jsbmb.2011.02.001.

Chumsri, S., Howes, T., Bao, T., Sabnis, G., Brodie, A., 2011b. Aromatase, aromatase inhibitors, and breast cancer. The Journal of Steroid Biochemistry and Molecular Biology https://doi.org/10.1016/j.jsbmb.2011.02.001.

Clemons, M., Goss, P., 2001. Estrogen and the risk of breast cancer. The New England Journal of Medicine 344:276–285. https://doi.org/10.1056/NEJM200101253440407.

Daldorff, S., Mathiesen, R.M.R., Yri, O.E., Ødegard, H.P., Geisler, J., 2017. Cotargeting of CYP-19 (aromatase) and emerging, pivotal signalling pathways in metastatic breast cancer. British Journal of Cancer https://doi.org/10.1038/bjc.2016.405.

Darden, T., York, D., Pedersen, L., 1993. Particle mesh Ewald: an N·log(N) method for Ewald sums in large systems. The Journal of Chemical Physics 98:10089. https://doi.org/10.1063/1.464397.

Debnath, A.K., 2002. Pharmacophore mapping of a series of 2,4-diamino-5-deazapteridine inhibitors of mycobacterium avium complex dihydrofolate reductase. Journal of Medicinal Chemistry 45:41–53. https://doi.org/10.1021/jm010360c.

Dias, D.A., Urban, S., Roessner, U., 2012. A historical overview of natural products in drug discovery. Metabolites 2:303–336. https://doi.org/10.3390/metabo2020303.

Dupont, S., Krust, A., Gansmuller, A., Dierich, A., Chambon, P., Mark, M., 2000. Effect of single and compound knockouts of estrogen receptors alpha (ERalpha) and beta (ERbeta) on mouse reproductive phenotypes. Development 127, 4277–4291.

Ghosh, D., Griswold, J., Erman, M., Pangborn, W., 2009. Structural basis for androgen specificity and oestrogen synthesis in human aromatase. Nature 457:219–223. https://doi.org/10.1038/nature07614.

Gillies, G.E., McArthur, S., 2010. Estrogen actions in the brain and the basis for differential action in men and women: a case for sex-specific medicines. Pharmacological Reviews 62:155–198. https://doi.org/10.1124/pr.109.002071.

Girard, R., Météreau, E., Thomas, J., Pugeat, M., Qu, C., Dreher, J.C., 2017. Hormone therapy at early post-menopause increases cognitive control-related prefrontal activity. Scientific Reports 7. https://doi.org/10.1038/srep44917.

Goss, P.E., Qi, S., Hu, H., Cheung, A.M., 2007. The effects of atamestane and toremifene alone and in combination compared with letrozole on bone, serum lipids and the uterus in an ovariectomized rat model. Breast Cancer Research and Treatment 103: 293–302. https://doi.org/10.1007/s10549-006-9381-y.

Hanamura, T., Hayashi, S., 2017. Overcoming aromatase inhibitor resistance in breast cancer: possible mechanisms and clinical applications. Breast Cancer https://doi.org/10.1007/s12282-017-0772-1.

Harada, N., 1997. Aberrant expression of aromatase in breast cancer tissues. The Journal of Steroid Biochemistry and Molecular Biology 61:175–184. https://doi.org/10.1016/S0960-0760(96)00200-2.

Hess, B., Bekker, H., Berendsen, H.J.C., Fraaije, J.G.E.M., 1997. LINCS: a linear constraint solver for molecular simulations. Journal of Computational Chemistry 18: 1463–1472. https://doi.org/10.1002/(SICI)1096-987X(199709)18:12<1463::AID-JCC4>3.0.CO;2-H.

Hong, Y., Chen, S., 2006. Aromatase inhibitors: structural features and biochemical characterization. Annals of the New York Academy of Sciences:237–251 https://doi.org/10.1196/annals.1386.022.

Humphrey, W., Dalke, A., Schulten, K., 1996. VMD: visual molecular dynamics. Journal of Molecular Graphics 14:33–38. https://doi.org/10.1016/0263-7855(96)00018-5.

Kang, H., Xiao, X., Huang, C., Yuan, Y., Tang, D., Dai, X., Zeng, X., 2018. Potent aromatase inhibitors and molecular mechanism of inhibitory action. European Journal of Medicinal Chemistry 143:426–437. https://doi.org/10.1016/j.ejmech.2017.11.057.

Katsila, T., Spyroulias, G.A., Patrinos, G.P., Matsoukas, M.-T., 2016. Computational approaches in target identification and drug discovery. Computational and Structural Biotechnology Journal 14:177–184. https://doi.org/10.1016/j.csbj.2016.04.004.

Knowlton, A.A., Lee, A.R., 2012. Estrogen and the cardiovascular system. Pharmacology & Therapeutics 135:54–70. https://doi.org/10.1016/j.pharmthera.2012.03.007.

Krege, J.H., Hodgin, J.B., Couse, J.F., Enmark, E., Warner, M., Mahler, J.F., Sar, M., Korach, K.S., Gustafsson, J.A., Smithies, O., 1998. Generation and reproductive phenotypes of mice lacking estrogen receptor beta. Proceedings of the National Academy of Sciences of the United States of America 95:15677–15682. https://doi.org/10.1073/pnas.95.26.15677.

Kumavath, R., Azad, M., Devarapalli, P., Tiwari, S., Kar, S., Barh, D., Azevedo, V., Kumar, A.P., 2016. Novel aromatase inhibitors selection using induced fit docking and extra precision methods: potential clinical use in ER-alpha-positive breast cancer. Bioinformation 12:324–331. https://doi.org/10.6026/97320630012324.

Langer, T., Hoffmann, R.D., 2006. Pharmacophore modelling: applications in drug discovery. Expert Opinion on Drug Discovery 1:261–267. https://doi.org/10.1517/17460441.1.3.261.

Lee, S., Barron, M.G., 2018. 3D-QSAR study of steroidal and azaheterocyclic human aromatase inhibitors using quantitative profile of protein–ligand interactions. Journal of Cheminformatics 10, 2. https://doi.org/10.1186/s13321-017-0253-8.

Lubahn, D.B., Moyer, J.S., Golding, T.S., Couse, J.F., Korach, K.S., Smithies, O., 1993. Alteration of reproductive function but not prenatal sexual development after insertional disruption of the mouse estrogen receptor gene. Proceedings of the National Academy of Sciences 90:11162–11166. https://doi.org/10.1073/pnas.90.23.11162.

Luqman, S., Meena, A., Singh, P., Kondratyuk, T.P., Marler, L.E., Pezzuto, J.M., Negi, A.S., 2012. Neoflavonoids and tetrahydroquinolones as possible cancer chemopreventive agents. Chemical Biology & Drug Design 80:616–624. https://doi.org/10.1111/j.1747-0285.2012.01439.x.

Lutter, M., Bahl, E., Hannah, C., Hofammann, D., Acevedo, S., Cui, H., McAdams, C.J., Michaelson, J.J., 2017. Novel and ultra-rare damaging variants in neuropeptide signaling are associated with disordered eating behaviors. PLoS One 12. https://doi.org/10.1371/journal.pone.0181556.

Lv, H.N., Wang, S., Zeng, K.W., Li, J., Guo, X.Y., Ferreira, D., Zjawiony, J.K., Tu, P.F., Jiang, Y., 2015. Anti-inflammatory coumarin and benzocoumarin derivatives from Murraya alata. Journal of Natural Products 78:279–285. https://doi.org/10.1021/np500861u.

Ma, C.X., Reinert, T., Chmielewska, I., Ellis, M.J., 2015. Mechanisms of aromatase inhibitor resistance. Nature Reviews. Cancer https://doi.org/10.1038/nrc3920.

Ma, Y., Li, H.-L., Chen, X.-B., Jin, W.-Y., Zhou, H., Ma, Y., Wang, R.-L., 2018. 3D QSAR pharmacophore based virtual screening for identification of potential inhibitors for CDC25B. Computational Biology and Chemistry 73:1–12. https://doi.org/10.1016/j.compbiolchem.2018.01.005.

Mangal, M., Sagar, P., Singh, H., Raghava, G.P.S., Agarwal, S.M., 2013. NPACT: naturally occurring plant-based anti-cancer compound-activity-target database. Nucleic Acids Research 41. https://doi.org/10.1093/nar/gks1047.

Maurizio, R., Andrea, C., Piero, V., 2002. Nonsteroidal aromatase inhibitors: recent advances. Medicinal Research Reviews 22:282–304. https://doi.org/10.1002/med.10010.

Mayhoub, A.S., Marler, L., Kondratyuk, T.P., Park, E.J., Pezzuto, J.M., Cushman, M., 2012. Optimization of the aromatase inhibitory activities of pyridylthiazole analogues of resveratrol. Bioorganic and Medicinal Chemistry 20:2427–2434. https://doi.org/10.1016/j.bmc.2012.01.047.

Mendelsohn, M.E., 2002. Protective effects of estrogen on the cardiovascular system. The American Journal of Cardiology 89:12–17. https://doi.org/10.1016/S0002-9149(02)02405-0.

Miller, W.R., 2004. Biological rationale for endocrine therapy in breast cancer. Best Practice & Research. Clinical Endocrinology & Metabolism https://doi.org/10.1016/S1521-690X(03)00044-7.

Miller, W.R., Larionov, A.A., 2012. Understanding the mechanisms of aromatase inhibitor resistance. Breast Cancer Research 14, 201. https://doi.org/10.1186/bcr2931.

Mirzaie, S., Chupani, L., Barzegari Asadabadi, E., Reza Shahverdi, A.R., Jamalan, M., 2013. Novel inhibitor discovery against aromatase through virtual screening and molecular dynamic simulation: a computational approach in drug design. EXCLI Journal 12.

Miyamoto, S., Kollman, P.A., 1992. Settle: an analytical version of the SHAKE and RATTLE algorithm for rigid water models. Journal of Computational Chemistry 13:952–962. https://doi.org/10.1002/jcc.540130805.

Mocanu, M.M., Nagy, P., Szöllosi, J., Mayence, A., 2015. Chemoprevention of breast cancer by dietary polyphenols. Molecules https://doi.org/10.3390/molecules201219864.

Musa, M., Cooperwood, J., Khan, M.O., 2008. A review of coumarin derivatives in pharmacotherapy of breast cancer. Current Medicinal Chemistry 15:2664–2679. https://doi.org/10.2174/092986708786242877.

Nakamura, T., Imai, Y., Matsumoto, T., Sato, S., Takeuchi, K., Igarashi, K., Harada, Y., Azuma, Y., Krust, A., Yamamoto, Y., Nishina, H., Takeda, S., Takayanagi, H., Metzger, D., Kanno, J., Takaoka, K., Martin, T.J., Chambon, P., Kato, S., 2007. Estrogen prevents bone loss via estrogen receptor alpha and induction of Fas ligand in osteoclasts. Cell 130:811–823. https://doi.org/10.1016/j.cell.2007.07.025.

Ntie-Kang, F., Zofou, D., Babiaka, S.B., Meudom, R., Scharfe, M., Lifongo, L.L., Mbah, J.A., Mbaze, L.M., Sippl, W., Efange, S.M.N., 2013. AfroDb: a select highly potent and diverse natural product library from African medicinal plants. PLoS One 8, e78085. https://doi.org/10.1371/journal.pone.0078085.

Numazawa, M., Kamiyama, T., Tachibana, M., Oshibe, M., 1996. Synthesis and structure-activity relationships of 6-substituted androst-4-ene analogs as aromatase inhibitors. Journal of Medicinal Chemistry 39:2245–2252. https://doi.org/10.1021/jm960047o.

O'Lone, R., Knorr, K., Jaffe, I.Z., Schaffer, M.E., Martini, P.G.V., Karas, R.H., Bienkowska, J., Mendelsohn, M.E., Hansen, U., 2007. Estrogen receptors alpha and beta mediate distinct pathways of vascular gene expression, including genes involved in mitochondrial electron transport and generation of reactive oxygen species. Molecular Endocrinology 21:1281–1296. https://doi.org/10.1210/me.2006-0497.

Park, W.-C., Jordan, V.C., 2002. Selective estrogen receptor modulators (SERMS) and their roles in breast cancer prevention. Trends in Molecular Medicine 8:82–88. https://doi.org/10.1016/S1471-4914(02)02282-7.

Parrinello, M., 1981. Polymorphic transitions in single crystals: a new molecular dynamics method. Journal of Applied Physics 52:7182. https://doi.org/10.1063/1.328693.

Prior, J.C., Seifert-Klauss, V.R., Giustini, D., Adachi, J.D., Kalyan, S., Goshtasebi, A., 2017. Estrogen-progestin therapy causes a greater increase in spinal bone mineral density than estrogen therapy — a systematic review and meta-analysis of controlled trials with direct randomization. Journal of Musculoskeletal & Neuronal Interactions 17, 146–154.

Rai, A., Aboumanei, M.H., Verma, S.P., Kumar, S., Raj, V., 2017. Molecular docking, pharmacophore, and 3D-QSAR approach: can adenine derivatives exhibit significant inhibitor towards Ebola virus? Open Medicinal Chemistry Journal 11:127–137. https://doi.org/10.2174/1874104501711010127.

Rampogu, S., Rampogu Lemuel, M., 2016. Network based approach in the establishment of the relationship between type 2 diabetes mellitus and its complications at the molecular level coupled with molecular docking mechanism. BioMed Research International 2016, 6068437. https://doi.org/10.1155/2016/6068437.

Rampogu, S., Son, M., Park, C., Kim, H.-H., Suh, J.-K., Lee, K., 2017. Sulfonanilide derivatives in identifying novel aromatase inhibitors by applying docking, virtual screening, and MD simulations studies. BioMed Research International 2017, 1–17.

Rampogu, S., Baek, A., Zeb, A., Lee, K.W., 2018a. Exploration for novel inhibitors showing back-to-front approach against VEGFR-2 kinase domain (4AG8) employing molecular docking mechanism and molecular dynamics simulations. BMC Cancer 18, 264. https://doi.org/10.1186/s12885-018-4050-1.

Rampogu, S., Son, M., Baek, A., Park, C., Rana, R.M., Zeb, A., Parameswaran, S., Lee, K.W., 2018b. Targeting natural compounds against HER2 kinase domain as potential anti-cancer drugs applying pharmacophore based molecular modelling approaches.

Computational Biology and Chemistry 74:327–338. https://doi.org/10.1016/j.compbiolchem.2018.04.002.

Riggs, B.L., 2000. The mechanisms of estrogen regulation of bone resorption. The Journal of Clinical Investigation https://doi.org/10.1172/JCI11468.

Sakkiah, S., Lee, K.W., 2012. Pharmacophore-based virtual screening and density functional theory approach to identifying novel butyrylcholinesterase inhibitors. Acta Pharmacologica Sinica 33:964–978. https://doi.org/10.1038/aps.2012.21.

Santen, R.J., Yue, W., Wang, J.P., 2015. Estrogen metabolites and breast cancer. Steroids https://doi.org/10.1016/j.steroids.2014.08.003.

Sini, V., Botticelli, A., Lunardi, G., Gori, S., Marchetti, P., 2017. Pharmacogenetics and aromatase inhibitor induced side effects in breast cancer patients. Pharmacogenomics 18. https://doi.org/10.2217/pgs-2017-0006.

Sonnet, P., Guillon, J., Enguehard, C., Dallemagne, P., Bureau, R., Rault, S., Auvray, P., Moslemi, S., Sourdaine, P., Galopin, S., Sérálini, G.E., 1998. Design and synthesis of a new type of non-steroidal human aromatase inhibitors. Bioorganic and Medicinal Chemistry Letters 8:1041–1044. https://doi.org/10.1016/S0960-894X(98)00157-7.

Sozen, T., Ozisik, L., Calik Basaran, N., 2017. An overview and management of osteoporosis. European Journal of Rheumatology 4:46–56. https://doi.org/10.5152/eurjrheum.2016.048.

Streicher, C., Heyny, A., Andrukhova, O., Haigl, B., Slavic, S., Schüler, C., Kollmann, K., Kantner, I, Sexl, V., Kleiter, M., Hofbauer, L.C., Kostenuik, P.J., Erben, R.G., 2017. Estrogen regulates bone turnover by targeting RANKL expression in bone lining cells. Scientific Reports 7. https://doi.org/10.1038/s41598-017-06614-0.

Subramanian, A., Salhab, M., Mokbel, K., 2008. Oestrogen producing enzymes and mammary carcinogenesis: a review. Breast Cancer Research and Treatment https://doi.org/10.1007/s10549-007-9788-0.

Tabatabaei-Malazy, O., Salari, P., Khashayar, P., Larijani, B., 2017. New horizons in treatment of osteoporosis. DARU Journal of Pharmaceutical Sciences 25:1–16. https://doi.org/10.1186/s40199-017-0167-z.

Thompson, E.A., Siiteri, P.K., 1974. Utilization of oxygen and reduced nicotinamide adenine dinucleotide phosphate by human placental microsomes during aromatization of androstenedione. The Journal of Biological Chemistry 249, 5364–5372.

Travis, R.C., Key, T.J., 2003. Oestrogen exposure and breast cancer risk. Breast Cancer Research https://doi.org/10.1186/bcr628.

Uysal, A., Zengin, G., Mollica, A., Gunes, E., Locatelli, M., Yilmaz, T., Aktumsek, A., 2016. Chemical and biological insights on Cotoneaster integerrimus: a new (-)-epicatechin source for food and medicinal applications. Phytomedicine 23:979–988. https://doi.org/10.1016/j.phymed.2016.06.011.

Väänänen, H.K., Härkönen, P.L., 1996. Estrogen and bone metabolism. Maturitas https://doi.org/10.1016/0378-5122(96)01015-8.

Van Der Spoel, D., Lindahl, E., Hess, B., Groenhof, G., Mark, A.E., Berendsen, H.J.C., 2005. GROMACS: fast, flexible, and free. Journal of Computational Chemistry https://doi.org/10.1002/jcc.20291.

Venugopala, K.N., Rashmi, V., Odhav, B., 2013. Review on natural coumarin lead compounds for their pharmacological activity. BioMed Research International https://doi.org/10.1155/2013/963248.

Yadav, M.R.A.M., Barmade, M.A., Tamboli, R.S., Murumkar, P.R., 2015. Developing steroidal aromatase inhibitors-an effective armament to win the battle against breast cancer. European Journal of Medicinal Chemistry https://doi.org/10.1016/j.ejmech.2015.09.038.

Yan, Y., Cheng, L., Chen, X., Wang, Q., Duan, M., Ma, J., Zhao, L., Jiang, X., Ai, J., 2017. Estrogen deficiency is associated with hippocampal morphological remodeling of early postmenopausal mice. Oncotarget https://doi.org/10.18632/oncotarget.15702.

Zarate, S., Stevnsner, T., Gredilla, R., 2017. Role of estrogen and other sex hormones in brain aging. Neuroprotection and DNA repair. Frontiers in Aging Neuroscience 9, 430.

Zengin, G., Aumeeruddy-Elafi, Z., Mollica, A., Yilmaz, M.A., Mahomoodally, M.F., 2018. In vitro and in silico perspectives on biological and phytochemical profile of three halophyte species—a source of innovative phytopharmaceuticals from nature. Phytomedicine 38:35–44. https://doi.org/10.1016/j.phymed.2017.10.017.

Zhao, H., Zhou, L., Shangguan, A.J., Bulun, S.E., 2016. Aromatase expression and regulation in breast and endometrial cancer. Journal of Molecular Endocrinology https://doi.org/10.1530/JME-15-0310.

Zoete, V., Cuendet, M.A., Grosdidier, A., Michielin, O., 2011. SwissParam: a fast force field generation tool for smallorganic molecules. Journal of Computational Chemistry 32: 2359–2368. https://doi.org/10.1002/jcc.21816.